Sensitivity Analysis for the Navier–Stokes Equations with Two-Equation Turbulence Models

Chang Sung Kim,* Chongam Kim,† and Oh Hyun Rho‡
Seoul National University, Seoul 151-742, Republic of Korea

Aerodynamic sensitivity analysis is performed for the Navier–Stokes equations, coupled with two-equation turbulence models using a discrete adjoint method and a direct differentiation method, respectively. Like the mean flow equations, the turbulence model equations are also hand differentiated to calculate accurately the sensitivity derivatives of flow quantities with respect to design variables in turbulent viscous flows. Both the direct differentiation code and the adjoint variable code adopt the same time integration scheme with the flow solver to solve the differentiated equations efficiently. The sensitivity codes are then compared with the flow solver in terms of solution accuracy, computing time, and computer memory requirements. The sensitivity derivatives obtained from the sensitivity codes with different turbulence models are compared with each other. Using two-equation turbulence models, it is observed that a usual assumption of constant turbulent eddy viscosity in adjoint methods may lead to inaccurate results in a case of turbulent flows involving strong shocks. The capability of the present sensitivity codes to treat complex geometry is successfully demonstrated by analyzing the flows over multielement airfoils on chimera overlaid grid systems.

Introduction

WITH the recent advances of computational power, design optimization methods using computational fluid dynamics (CFD) became popular tools in aerodynamic design. Before the actual design process, an accurate and efficient flow solver is required for the computation of pressure distribution and aerodynamic loads such as lift, drag, and pitching moment, which are used in an objective function to be minimized. Derivatives with respect to each design variable may be obtained by the finite difference method. It is, however, too expensive to compute the flowfield iteratively with the incremented values of a design variable for complex two-dimensional or three-dimensional problems. In addition, this method is so sensitive to the step size of a design variable that it sometimes provides inaccurate signs or values of sensitivity derivatives.[1,2] Therefore, more robust techniques have been proposed using the direct differentiation methods and the adjoint variable methods.[2−11] The direct differentiation methods provide computed derivatives that are coincident with finite differenced derivatives and are useful when the number of design variables is smaller than that of the objective function and constraints. On the other hand, the adjoint variable methods are more advantageous for their capability to compute the gradients of the objective function and constraints when the number of design variables is larger than that of the objective function and constraints. The direct differentiation methods use the discrete form of the flow equations, and the adjoint variable methods adopt the formulation of the gradient in either a discrete or a continuous approach. In the discrete approach, which is used in the present work, the discretized governing equations are differentiated with respect to design variables, whereas the adjoint equations are first differentiated and then discretized in the continuous approach.[7,8]

To treat high-Reynolds-number flows accurately, it is necessary to incorporate the effect of turbulence in differentiating the governing equations. It is, however, very difficult to fully hand differentiate the governing equations including the viscous terms and turbulence terms. Some software tools such as automatic differentiation[5,6,9,10] are used for the Navier–Stokes equations with a turbulence model. However, this approach is generally less efficient, in terms of computing time and computer memory, than hand-differentiation codes.[5,11]

In the present work, the Navier–Stokes equations coupled with two-equation turbulence models are fully differentiated by hand. Among most popular two-equation turbulence models,[12−15] the k–ω shear stress transport (SST) model proposed by Menter[14,15] is mainly used and then compared with the k–ω model of Wilcox[12,13] and the standard k–ε model.[15] Like the mean flow equations, the turbulence model equations are also hand differentiated to compute accurately the sensitivity derivatives of flow quantities with respect to design variables in turbulent flows. Two codes, using a discrete adjoint method and a direct differentiation method, respectively, are developed for the aerodynamic sensitivity analysis. The aerodynamic sensitivity analysis direct differentiation (ASADD) code and the aerodynamic sensitivity analysis adjoint variable (ASAAV) code are then carefully validated for a turbulent flow over the Royal Aircraft Establishment (RAE) 2822 transonic airfoil. The derivatives from the sensitivity codes are compared with the finite difference derivatives for non-geometric flow design variables and a geometric design variable.

A usual assumption of constant turbulent eddy viscosity in the adjoint variable methods has been previously used in aerodynamic design optimizations.[7,8] Recently, the accuracy of this assumption in turbulent flows was reported using a one-equation turbulence model on unstructured grids and an algebraic turbulence model in Refs. 2 and 11, respectively. In the present work, the feasibility of this assumption is studied by comparing the sensitivity derivatives in three different flow regimes: a low-speed subsonic flow over the NACA 4412 airfoil and subsonic and transonic turbulent flows over the RAE 2822 airfoil.

To demonstrate the capability to handle complex geometry in turbulent flows, sensitivity analysis codes using the chimera grid scheme[16] are developed and validated for the flows over two- and three-element airfoils, the National Aerospace Laboratory (NLR) 7301 airfoil with flap and the General Aviation Wing (GAW)-1 high-lift airfoil with a leading-edge slat and a trailing-edge flap.

*Graduate Research Assistant, Department of Aerospace Engineering. Student Member AIAA.

†Assistant Professor, Department of Aerospace Engineering. Member AIAA.

‡Professor, Department of Aerospace Engineering. Senior Member AIAA.

Numerical Background

Governing Equations and Numerical Approach

The governing equations are the two-dimensional, unsteady, compressible Navier–Stokes equations coupled with the k–ω SST turbulence model,[15] which can be written in a conservation law form as

---

$$\frac{\partial \rho}{\partial t} + \frac{\partial}{\partial x_j}(\rho u_j) = 0$$

$$\frac{\partial}{\partial t}(\rho u_i) + \frac{\partial}{\partial x_j}(\rho u_j u_i) = -\frac{\partial p}{\partial x_i} + \frac{\partial \hat{\tau}_{ij}}{\partial x_j}$$

$$\frac{\partial \rho E}{\partial t} + \frac{\partial}{\partial x_j}(\rho E u_j) = -\frac{\partial p u_j}{\partial x_j} + \frac{\partial}{\partial x_j}[u_i \hat{\tau}_{ij} - q_j]$$

$$\frac{\partial \rho k}{\partial t} + \frac{\partial}{\partial x_j}(\rho k u_j) = \tau_{ij}\frac{\partial u_i}{\partial x_j} - \beta * \rho\omega k + \frac{\partial}{\partial x_j}\left[(\mu + \sigma_k \mu_T)\frac{\partial k}{\partial x_j}\right]$$

$$\frac{\partial \rho \omega}{\partial t} + \frac{\partial}{\partial x_j}(\rho\omega u_j) = \frac{\gamma}{\nu_T}\tau_{ij}\frac{\partial u_i}{\partial x_j} - \beta\rho\omega^2$$
$$+ \frac{\partial}{\partial x_j}\left[(\mu + \sigma_\omega \mu_T)\frac{\partial \omega}{\partial x_j}\right] + 2(1 - F_1)\rho\sigma_{\omega 2}\frac{1}{\omega}\frac{\partial k}{\partial x_j}\frac{\partial \omega}{\partial x_j} \quad (1)$$

where E represents the total energy and $\hat{\tau}_{ij}$ are composed of molecular and Reynolds stresses, defined as

$$\hat{\tau}_{ij} = 2\mu\left(S_{ij} - \frac{S_{kk}\delta_{ij}}{3}\right) + \tau_{ij}$$

$$\tau_{ij} = 2\mu_T\left(S_{ij} - \frac{S_{kk}\delta_{ij}}{3}\right) - \frac{2\rho k\delta_{ij}}{3}, \qquad S_{ij} = \frac{1}{2}\left(\frac{\partial u_i}{\partial x_j} + \frac{\partial u_j}{\partial x_i}\right) \quad (2)$$

and where q_j is the total heat-flux rate defined as

$$q_j = -\left(\frac{\gamma}{\gamma - 1}\right)\left(\frac{\mu}{Pr} + \frac{\mu_T}{Pr_T}\right)\frac{\partial T}{\partial x_j} \quad (3)$$

The turbulent eddy viscosity is defined as

$$\mu_T = 0.31\rho k/\max(0.31\omega; \Omega F_2) \quad (4)$$

where F_1 and F_2 are turbulence functions and Ω is the absolute value of vorticity. More details about the turbulence models can be found in Refs. 14, 15, and 17. The equation of state is introduced to complete the set of the governing equations as

$$p = \rho(\gamma - 1)\left[E - \tfrac{1}{2}u_i u_i - k\right] \quad (5)$$

The governing equations are transformed in generalized coordinates and are solved with a finite volume method. With a backward Euler implicit method, the governing equations are discretized in time and linearized in delta form as

$$\left(\frac{I}{J\Delta t} + \left[\frac{\partial R}{\partial Q}\right]^n\right)\Delta Q = -R^n \quad (6)$$

where J is the Jacobian of transformation, R is the residual of the steady-state flow equations, and Q is the six-element vector of conservative variables $(\rho, \rho u, \rho v, \rho e, \rho k, \rho\omega)^T$.

For the calculation of the residual, convective terms are upwind differenced based on Roe's flux difference splitting (FDS) scheme,[18] and viscous terms are central differenced. A MUSCL approach using a third-order interpolation is used to obtain a higher order of spatial accuracy.[19] The third order of spatial accuracy is kept in all calculations. For a temporal integration, the Yoon and Kwak LU-SGS scheme[20] is adopted to solve efficiently Eq. (6). Wall boundary conditions are applied explicitly with the nonslip condition. For inflow and outflow boundaries, characteristic conditions based on one-dimensional Riemann invariants are imposed. For the chimera grid scheme, a bilinear interpolation that is known to be robust and easy to implement is adopted for the hole-cutting boundary.[17]

Sensitivity Analysis

The discrete residual of the steady-state flow equations can be written as

$$\{R\} = \{R(Q, X, D)\} = \{0\} \quad (7)$$

where X is the computational grid position and D is the vector of design variables. Similarly, the vector of the aerodynamic objective function F to be either minimized or maximized is also dependent on Q, X, and D as

$$\{F\} = \{F(Q, X, D)\} \quad (8)$$

In the direct differentiation method, the sensitivity derivatives of the aerodynamic functions are calculated by directly differentiating Eqs. (7) and (8) with respect to D as

$$\left\{\frac{dR}{dD}\right\} = \left[\frac{\partial R}{\partial Q}\right]\left\{\frac{dQ}{dD}\right\} + \left[\frac{\partial R}{\partial X}\right]\left\{\frac{dX}{dD}\right\} + \left\{\frac{\partial R}{\partial D}\right\} = \{0\} \quad (9)$$

$$\left\{\frac{dF}{dD}\right\} = \left[\frac{\partial F}{\partial Q}\right]^T\left\{\frac{dQ}{dD}\right\} + \left[\frac{\partial F}{\partial X}\right]^T\left\{\frac{dX}{dD}\right\} + \left\{\frac{\partial F}{\partial D}\right\} \quad (10)$$

The geometric sensitivity vector $\{dX/dD\}$ can be calculated by differentiating the grid generation code. In the present work, the finite difference approximation is applied for simplicity. The solution vector $\{dQ/dD\}$ is calculated by applying the same backward Euler implicit method as the flow solver:

$$\left(\frac{I}{J\Delta t} + \left[\frac{\partial R}{\partial Q}\right]\right)\Delta\left\{\frac{dQ}{dD}\right\} = -\left\{\frac{dR}{dD}\right\}^m$$

$$\left\{\frac{dQ}{dD}\right\}^{m+1} = \left\{\frac{dQ}{dD}\right\}^m + \Delta\left\{\frac{dQ}{dD}\right\} \quad (11)$$

The flux Jacobian $[\partial R/\partial Q]$ in Eq. (11) is given by a steady-state solution from the flow solver. Equation (11) is then efficiently solved using the LU-SGS scheme, which is adopted for the flow equations. All boundary conditions including the hole-cutting boundary conditions for the chimera grid scheme are given by directly differentiating the boundary-condition equations for the flow solver.

In the adjoint variable method, the sensitivity derivatives of the aerodynamic functions are obtained by combining Eqs. (9) and (10) as

$$\left\{\frac{dF}{dD}\right\} = \left\{\frac{\partial F}{\partial Q}\right\}^T\left\{\frac{dQ}{dD}\right\} + \left\{\frac{\partial F}{\partial X}\right\}^T\left\{\frac{dX}{dD}\right\} + \left\{\frac{\partial F}{\partial D}\right\}$$
$$+ \Lambda^T\left(\left[\frac{\partial R}{\partial Q}\right]\left\{\frac{dQ}{dD}\right\} + \left[\frac{\partial R}{\partial X}\right]\left\{\frac{dX}{dD}\right\} + \left\{\frac{\partial R}{\partial D}\right\}\right) \quad (12)$$

where Λ represents the six-element adjoint vector of Lagrangian multipliers $(\lambda_1, \lambda_2, \lambda_3, \lambda_4, \lambda_5, \lambda_6)^T$ corresponding to the conservative variables $(\rho, \rho u, \rho v, \rho e, \rho k, \rho\omega)^T$. Rearranging Eq. (12) yields the following equation:

$$\left\{\frac{dF}{dD}\right\} = \left\{\frac{\partial F}{\partial X}\right\}^T\left\{\frac{dX}{dD}\right\} + \left\{\frac{\partial F}{\partial D}\right\}$$
$$+ \Lambda^T\left(\left[\frac{\partial R}{\partial X}\right]\left\{\frac{dX}{dD}\right\} + \left\{\frac{\partial R}{\partial D}\right\}\right)$$
$$+ \left(\left\{\frac{\partial F}{\partial Q}\right\}^T + \Lambda^T\left[\frac{\partial R}{\partial Q}\right]\right)\left\{\frac{dQ}{dD}\right\} \quad (13)$$

Without evaluating the vector $\{dQ/dD\}$, the sensitivity derivatives of the aerodynamic functions can be calculated as

$$\left\{\frac{dF}{dD}\right\} = \left\{\frac{\partial F}{\partial X}\right\}^T \left\{\frac{dX}{dD}\right\} + \left\{\frac{\partial F}{\partial D}\right\}$$

$$+ \Lambda^T \left(\left[\frac{\partial R}{\partial X}\right]\left\{\frac{dX}{dD}\right\} + \left\{\frac{\partial R}{\partial D}\right\}\right) \quad (14)$$

if and only if the arbitrary vector Λ satisfies the following adjoint equation:

$$\left[\frac{\partial R}{\partial Q}\right]^T \Lambda + \left\{\frac{\partial F}{\partial Q}\right\} = \{0\}^T \quad (15)$$

To obtain the solution vector Λ in Eq. (15), the backward Euler implicit method with pseudotime marching is used as

$$\left(\frac{I}{J\Delta\tau} + \left[\frac{\partial R}{\partial Q}\right]^T\right)\Delta\Lambda = -\left[\frac{\partial R}{\partial Q}\right]^T \Lambda^m - \left\{\frac{\partial F}{\partial Q}\right\}^T$$

$$\Lambda^{m+1} = \Lambda^m + \Delta\Lambda \quad (16)$$

The transposed flux Jacobian $[\partial R/\partial Q]^T$ on the right-hand side of Eq. (16) is a very large banded matrix requiring a large computer memory. To reduce the memory overhead, each element of the adjoint vector Λ is multiplied to the corresponding element of $[\partial R/\partial Q]^T$ in the present work. This requires the recalculation of $[\partial R/\partial Q]^T$ at every iteration, and the extra computation time is necessary. Nevertheless, this technique is preferable to avoid prohibitive memory requirements for large two-dimensional problems and all three-dimensional problems.[2,5,11] Boundary conditions in the adjoint variable methods are given from Eq. (15) as

$$\left[\frac{\partial R}{\partial Q}\right]^T \Lambda + \left[\frac{\partial R_B}{\partial Q}\right]^T \Lambda_B + \left\{\frac{\partial F}{\partial Q}\right\}^T = \{0\}^T \quad (17a)$$

$$\left[\frac{\partial R}{\partial Q_B}\right]^T \Lambda + \left[\frac{\partial R_B}{\partial Q_B}\right]^T \Lambda_B + \left\{\frac{\partial F}{\partial Q_B}\right\}^T = \{0\}^T \quad (17b)$$

where subscript B represents the boundary cells. Because $[\partial R_B/\partial Q_B]^T$ in Eq. (17b) is an identity matrix, Λ_B is calculated as

$$\Lambda_B = -\left[\frac{\partial R}{\partial Q_B}\right]^T \Lambda - \left\{\frac{\partial F}{\partial Q_B}\right\}^T \quad (18)$$

and $[\partial R/\partial Q]^T \Lambda$ is obtained by substituting Λ_B into Eq. (17a).

For the chimera grid scheme, a bilinear interpolation is adopted for the hole-cutting boundary. These boundary conditions also need to be carefully treated. The discrete residual at the fringe cells of the main grid can be written as

$$\{R_F^M\} = \{R_F^M(Q_F^M, Q^S)\} = \{0\} \quad (19)$$

Likewise, the discrete residual at the fringe cells of the subgrid can be written as

$$\{R_F^S\} = \{R_F^S(Q_F^S, Q^M)\} = \{0\} \quad (20)$$

where the subscript F represents fringe cells and the superscript M and S represent the main grid and subgrid domain, respectively. Then the equations for the boundary conditions at the fringe cells can be derived from Eqs. (15), (19), and (20) as

$$\left[\frac{\partial R^M}{\partial Q^M}\right]^T \Lambda^M + \left[\frac{\partial R_F^S}{\partial Q^M}\right]^T \Lambda_F^S + \left\{\frac{\partial F^M}{\partial Q^M}\right\}^T = \{0\}^T \quad (21a)$$

$$\left[\frac{\partial R^S}{\partial Q^S}\right]^T \Lambda^S + \left[\frac{\partial R_F^M}{\partial Q^S}\right]^T \Lambda_F^M + \left\{\frac{\partial F^S}{\partial Q^S}\right\}^T = \{0\}^T \quad (21b)$$

and Λ_F^S and Λ_F^M of Eqs. (21a) and (21b) are given by the following equations:

$$\Lambda_F^S = -\left[\frac{\partial R^S}{\partial Q_F^S}\right]^T \Lambda^S - \left\{\frac{\partial F^S}{\partial Q_F^S}\right\}^T \quad (21c)$$

$$\Lambda_F^M = -\left[\frac{\partial R^M}{\partial Q_F^M}\right]^T \Lambda^M - \left\{\frac{\partial F^M}{\partial Q_F^M}\right\}^T \quad (21d)$$

Results and Discussion

Direct Differentiation (DD) Method

The flow over the RAE 2822 transonic airfoil is tested to validate the direct differentiation (DD) code at a Mach number of 0.73, a Reynolds number of 6.5×10^6, and an angle of attack of 2.79 deg. A 129×65 hyperbolic grid is used with the wall spacing of 1×10^{-5} chord. The computed surface pressure coefficients from the flow solver using the $k–\omega$ SST model[14,15] are compared with those from the $k–\omega$ model,[12,13] the standard $k–\varepsilon$ model,[15] and the experimental data[21] in Fig. 1.
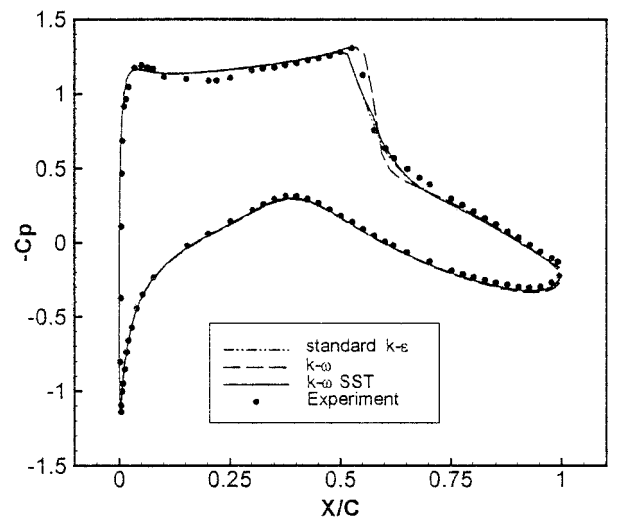
The consistency of the derivatives from the DD code with the finite difference derivatives is demonstrated in two cases for a nongeometric flow design variable and a geometric design variable. In the first case, angle of attack α is given as a flow design variable. Figure 2 shows the contour lines of the pressure derivative with respect to angle of attack obtained from the finite difference approximation and the DD. The derivatives of the aerodynamic load coefficients such as lift, drag, and pitching moment are all obtained from the same computed result and compared with the finite difference (FD) derivatives in Table 1. Two perturbation sizes of 1×10^{-5} and 1×10^{-7} are chosen, and the FD derivatives are calculated by central difference approximation. The derivatives from the two step sizes coincide with the results obtained from the DD code.

In the second case, geometric change is given by a Hicks–Henne function as

$$F(x) = \sin^3[\pi x(\ell n 0.5/\ell n 0.6)] \quad (22)$$

Table 1   Sensitivity derivatives of load coefficients with respect to angle of attack
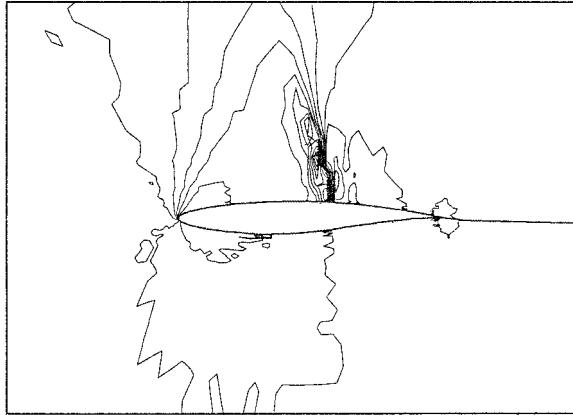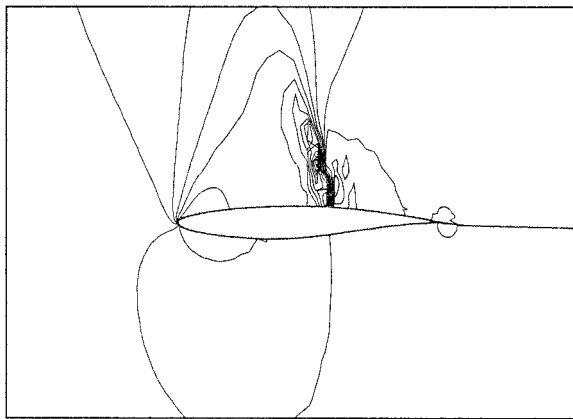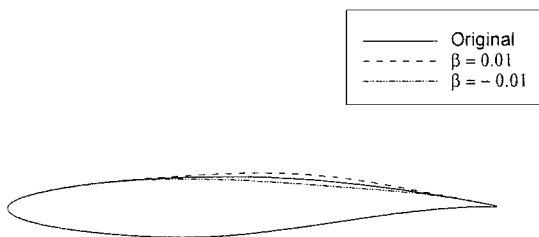
α	FD		DD
	$\Delta\alpha = 10^{-5}$	$\Delta\alpha = 10^{-7}$	
C_L	8.741617	8.7416	8.7416
C_D	0.593011	0.5929	0.5929
C_M	0.002292	0.0023	0.0023

Fig. 1 Surface pressure coefficients over the RAE 2822 airfoil at $\alpha = 2.79$ deg, $M = 0.73$, and $Re = 6.5 \times 10^6$.

Table 2   Sensitivity derivatives of load coefficients with respect to geometric change

β	FD		DD
	$\Delta\beta = 10^{-5}$	$\Delta\beta = 10^{-7}$	
C_L	10.200000	10.2300	10.2380
C_D	−0.165799	−0.1659	−0.1645
C_M	−2.795491	−2.7955	−2.8034

Table 3   Sensitivity derivatives of lift coefficient

$\partial C_L / \partial D$	FD	DD	AV
M_∞	2.3110	2.3110	2.3110
α	8.7416	8.7416	8.7416
β	10.2300	10.2380	10.2380

a) Finite difference approximation

b) Direct differentiation

Fig. 2   Contour lines of pressure derivatives with respect to angle of attack, $\mathrm{d}p/\mathrm{d}\alpha$, over the RAE 2822 airfoil.

a) Finite difference approximation

b) Direct differentiation

Fig. 4   Contour lines of pressure derivatives with respect to geometric change, $\mathrm{d}p/\mathrm{d}\beta$, on the upper surface of the RAE 2822 airfoil.

	Original
	$\beta = 0.01$
	$\beta = -0.01$

Fig. 3   Geometric changes on the upper surface of the RAE 2822 airfoil due to a design variable β.

and the upper surface geometry of the airfoil is changed using Eq. (22) as

$$y = y_0 + \beta F(x) \qquad (23)$$

where y_0 represents the original geometry. As depicted in Fig. 3, β is a geometric design variable of concern whose value is chosen as 1×10^{-7}.

As in the first case, the sensitivity derivatives of the aerodynamic lift, drag, and pitching moment coefficients are compared with the FD derivatives in Table 2. The FD derivatives with the perturbation sizes of 1×10^{-5} and 1×10^{-7} are calculated using the central difference approximation. Unlike the first case, the FD is slightly sensitive to the perturbation size. The derivatives using the step size of 1×10^{-7} coincide well with the DD results. In the rest of the present paper, all of the FD calculations are performed with the step size of 1×10^{-7}. Figure 4 shows the contour lines of the pressure derivative with respect to geometric change obtained from the FD approximation and the DD.

Adjoint Variable Method

To validate the adjoint variable (AV) code, the flow over the RAE 2822 airfoil is also tested under the same flow conditions as in the case of the DD code. The sensitivity derivatives are computed for the lift coefficient with respect to the freestream Mach number, angle of attack, and geometric change using Eq. (23). The sensitivity derivatives of the three design variables are all obtained from the same computed result for the lift coefficient. The sensitivity derivatives from the AV code are compared with those from the DD code as well as the FD derivatives in Table 3. The derivatives from the AV code coincide with the DD results. Although Lagrangian multipliers have no physical meaning in the AV methods, the streamlines of AV vector (λ_2, λ_3) corresponding to the conservative variable vector $(\rho u, \rho v)$ are presented for the code validation in Fig. 5.

In the second case, the sensitivity derivatives are computed for the drag coefficient with respect to the freestream Mach number, angle of attack, and geometric change. The sensitivity derivatives

Table 4   Sensitivity derivatives for drag coefficient

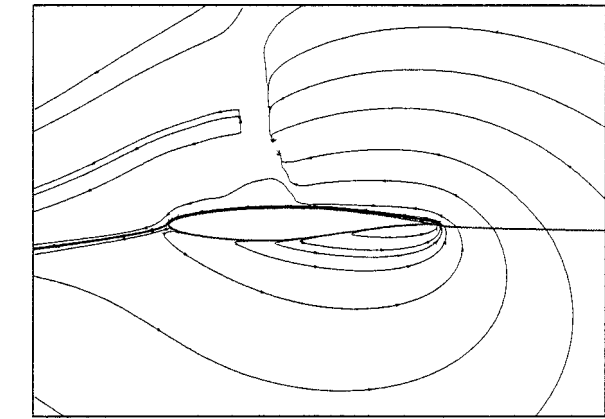| $\partial C_D/\partial D$	FD	DD	AV
M_∞	0.4573	0.4573	0.4573
α	0.5929	0.5929	0.5929
β	−0.1659	−0.1645	−0.1646

Fig. 5   Streamlines of adjoint vector (λ_2, λ_3) over the RAE 2822 airfoil.

Fig. 6   Convergence history of the sensitivity analysis codes.

Table 5   Effects of turbulence models on sensitivity derivatives

$\partial C_L/\partial D$	DD	AV
	$k-\omega$, SST	
α	8.7416	8.7416
β	10.2380	10.2380
	$k-\varepsilon$	
α	10.2270	10.2270
β	7.7078	7.7078
	$k-\omega$	
α	8.9427	8.9427
β	2.6211	2.6211

Table 6   Sensitivity derivatives of load coefficients for NACA 4412 airfoil[a]

Derivative	DD	AV	AV (μ_T = const)
$\dfrac{dC_L}{d\alpha}$	6.3948	6.3948	6.2855
$\dfrac{dC_L}{d\beta}$	2.3252	2.3252	2.5451
$\dfrac{dC_D}{d\alpha}$	0.0544	0.0544	0.0535
$\dfrac{dC_D}{d\beta}$	0.0388	0.0388	0.0337

[a] $M = 0.3$, $Re = 2.51 \times 10^6$, 2.0 deg.

tions as in the earlier case. The sensitivity derivatives are computed for the lift coefficient with respect to angle of attack and geometric change as shown in Fig. 3. For each turbulence model, the derivatives obtained from the AV code coincide with the DD results.

Note, however, that the $k-\omega$ model yields a noticeable difference with the other two models in case of geometric change β. This can be explained from the result that the shock position predicted by the $k-\omega$ model is different from the results of the other two models as shown in Fig. 1. The geometric change is applied to the region where a strong shock wave develops as shown in Fig. 4. The effects of turbulence models on the prediction of aerodynamic load coefficients over single- and multielement airfoils were previously reported in Ref. 17.

Feasibility Study of Constant Eddy Viscosity Assumption

The differentiation of a one- or two-equation turbulence model is difficult to implement because of the complicated terms such as the turbulence production and dissipation term. To reduce the effort to obtain the differentiation of the turbulence transport equations, the turbulent eddy viscosity μ_T is often assumed to be constant in the AV methods.[7,8] In other words, the derivatives of μ_T with respect to the conservative variables Q are set to zero. It also saves the computing time because the turbulence model equations in Eq. (16) do not need to be solved. This assumption, however, may not guarantee the accuracy of the derivatives because it neglects the contribution of the turbulence model to the flow analysis.[2,11]

To examine this assumption more closely, the sensitivity derivatives from the AV code using the $k-\omega$ SST model, with and without the differentiation of the eddy viscosity, are compared in three different flowfields: a low-speed subsonic flow over the NACA 4412 airfoil, a subsonic flow over the RAE 2822 airfoil, and a transonic turbulent flow over the RAE 2822 airfoil.

For the NACA 4412 airfoil, the flow conditions are given by a freestream Mach number of 0.3, a Reynolds number of 2.51×10^6, and an angle of attack of 2.0 deg. The sensitivity derivatives with constant eddy viscosity assumption show slight differences with the results of the DD code and the complete AV code ($\partial \mu_T/\partial Q \neq 0$) as shown in Table 6. For the design variable of angle of attack α, the deviations are less than about 2% and are about 9–13% for geometric change β.

from the AV code are compared with the FD derivatives and the DD results in Table 4, which shows good agreement between them.

The convergence history of the sensitivity analysis codes is shown and compared with that of the flow solver in Fig. 6. The residuals of the flow solver and the sensitivity codes are reduced to machine accuracy zero. The DD code shows quite a similar convergence characteristics to the flow solver. As mentioned before, each element of the adjoint vector Λ in Eq. (16) is multiplied to the corresponding element of $[\partial R/\partial Q]^T$ due to the memory requirement. Thus, the AV code requires additional computing time for the recalculation of $[\partial R/\partial Q]^T$ at every iteration. In this case, the AV code requires about 4.8 times more computing time than the flow solver, whereas the DD code requires about 1.4 times more. With regard to the computer memory, the AV code requires about 2.3 times more memory than the flow solver, whereas the DD code requires about 1.9 times more.

Effects of Turbulence Models

To study the effects of turbulence models, the sensitivity derivatives from the $k-\omega$ SST model are compared in Table 5 with those from the standard $k-\varepsilon$ and $k-\omega$ models under the same flow condi-

Table 7   Sensitivity derivatives of lift coefficient
for RAE 2822 airfoil[a]

M_∞	$\partial C_L/\partial D$	AV	AV (μ_T = const)
		k–ω, SST	
0.63	α	8.6373	8.3706
0.63	β	3.5869	3.6923
0.73	α	8.7416	4.4664
0.73	β	10.2380	13.8750
		k–ε	
0.73	α	10.2270	7.4277
0.73	β	7.7078	9.7723
		k–ω	
0.73	α	8.9427	7.3045
0.73	β	2.6211	1.9089

[a]$Re = 6.5 \times 10^6$, $\alpha = 2.79$ deg.

a) $\partial\mu_L/\partial\rho$ contour: $\partial\mu_T/\partial\rho = 0$ assumed

b) $\partial(\mu_L + \mu_T)/\partial\rho$ contour

Fig. 7   Effects of constant eddy viscosity assumption at a freestream Mach number of 0.73.

However, Table 7 shows clearly that this assumption may lead to more serious deviations for turbulent flows involving a strong shock. Although a shock-induced separation does not occur, a strong shock develops on the upper surface of the airfoil when the freestream Mach number is 0.73. In this case, the deviations reach up to about 20–50% for the design variable of angle of attack and about 35–65% for geometric change. Much like the k–ω SST model, the standard k–ε and the k–ω models also show similar behavior in predicting the sensitivity derivatives with the assumption of constant turbulent eddy viscosity.

The turbulent eddy viscosity μ_T is combined with the laminar viscosity μ in the governing equations as written in Eqs. (2) and (3). To see the effects of constant eddy viscosity assumption, the contour lines of the laminar and total viscosity derivatives with respect to density are compared on the same contour level in Fig. 7 in the case of

Table 8   Sensitivity derivatives of lift
coefficient for two-element airfoil

$\partial C_L/\partial D$	DD	AV
M_∞	0.0810	0.0810
α	7.9886	7.9886
Main airfoil	1.7736	1.7736
Flap	−11.981	−11.981

Fig. 8   Surface pressure coefficients over the NLR 7301 with flap at $\alpha = 6.0$ deg, $M = 0.185$, and $Re = 2.51 \times 10^6$.

a freestream Mach number of 0.73. As shown in Fig. 7b, the turbulent eddy viscosity derivative has a large value in the turbulent boundary layer and becomes much larger in the downstream adverse pressure gradient region after the shock wave. Thus, a constant eddy viscosity assumption would yield a significant error because it neglects the very large value of the turbulent eddy viscosity derivative, especially in the downstream adverse pressure gradient region after the shock wave, which directly influences the variation of aerodynamic load coefficients. Therefore, note that the contribution of turbulence must be taken into account for the accurate calculations of the sensitivity derivatives in highly turbulent flows involving strong shocks.

Sensitivity Analysis on Chimera Grid
To treat complex geometry such as two- and three-element airfoils, aerodynamic sensitivity analyses are applied on chimera grid systems using the DD code and the complete AV code based on the k–ω SST model.

In the case of a two-element airfoil, the flow over the NLR 7301 airfoil with a 32%c flap is tested at a Mach number of 0.3 and a Reynolds number of 3.0×10^6. The flap is positioned with a deflection angle of 20 deg, an overlap of 5.3%c, and a gap of 2.6%c. A 249×81 hyperbolic grid for the basic airfoil and a 125×41 grid for the flap are used with the wall spacing on the order of 10^{-6} chord. The computed surface pressure coefficient using the k–ω SST model is compared with the experimental data[22] at a Mach number of 0.185, a Reynolds number of 2.51×10^6, and an angle of attack of 6.0 deg in Fig. 8. The sensitivity derivatives of lift coefficient with respect to the freestream Mach number, angle of attack, and geometric changes of the main airfoil and flap are presented in Table 8. The streamlines of the velocity derivative from the DD code with respect to angle of attack are shown in Fig. 9. For the geometric changes of the main airfoil, the upper surface is deformed using Eq. (23), whereas both the upper and lower surfaces of the flap are changed using the following equation:

$$y = y_0 + \gamma F(x), \qquad F(x) = \sin^3[\pi x(\ell_n 0.5/\ell_n 0.4)] \qquad (24)$$

where y_0 represents the original flap geometry. As shown in Fig. 10, γ is the design variable of concern, whose value is 1×10^{-7}. The streamlines of the velocity derivative with respect to the flap geometric change are shown in Fig. 11.

The convergence history of the sensitivity analysis codes using the chimera grid scheme is shown and compared with that of the

Fig. 9   Streamlines of velocity derivatives with respect to angle of attack ($du/d\alpha$, $d\nu/d\alpha$) over the NLR 7301 airfoil with flap at $\alpha = 1.0$ deg, $M = 0.3$, and $Re = 3.0 \times 10^6$.
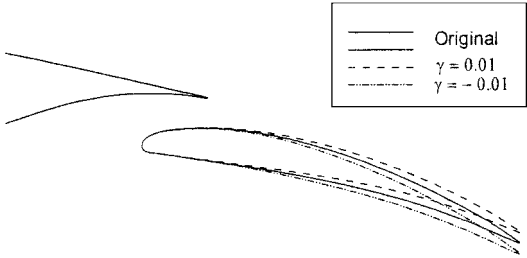

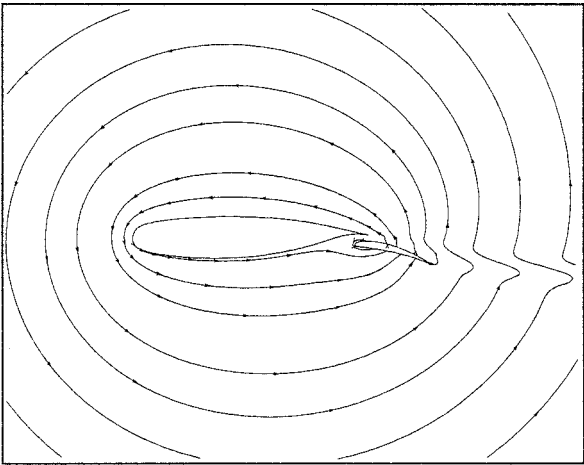Fig. 10   Geometric change near the trailing edge of the flap due to a design variable γ.

Fig. 11   Streamlines of velocity derivatives with respect to geometric change ($du/d\beta$, $d\nu/d\beta$) on the flap of the NLR 7301 airfoil.

Fig. 12   Convergence history of the sensitivity analysis codes on a chimera grid.

Fig. 13   Surface pressure coefficients over the GAW-1 high-lift airfoil at $\alpha = 12.0$ deg, $M = 0.15$, and $Re = 0.62 \times 10^6$.

Fig. 14   Geometric change near the trailing edge of the slat due to a design variable γ.

flow solver in Fig. 12. Much like the case of single airfoil, the DD code shows quite a similar convergence characteristics with the flow solver. In this case, the AV code requires about 5 times more computing time than the flow solver, whereas the DD code requires about 1.5 times more. With regard to the computer memory, the AV code requires about 2 times more memory than the flow solver, whereas the DD code requires about 1.6 times more.

In three-element airfoil case, the flow over the NASA GAW-1 high-lift airfoil with a $15\%c$ leading-edge slat and a $29\%c$ trailing-edge flap is tested at an angle of attack of 2.0 deg. The slat is positioned with a deflection angle of -42 deg, an overlap of $1.5\%c$, and a gap of $1.5\%c$, whereas the flap is positioned with a deflection angle of 30 deg, an overlap of $0.0\%c$, and a gap of $2.5\%c$. Figure 13

shows the computed surface pressure coefficients compared with the experimental data[23] at a Mach number of 0.15, a Reynolds number of 0.65×10^6, and an angle of attack of 12.0 deg.

The sensitivity derivatives of lift coefficient with respect to the freestream Mach number, angle of attack, and geometric changes of three elements are presented in Table 9. For the geometric change of the slat, both the upper and lower surfaces of the slat are changed using Eq. (24) as depicted in Fig. 14. The streamlines of the velocity derivative with respect to the slat geometric change are presented on the chimera grid in Fig. 15. As in two-element airfoil case, the